Study of rare baryonic-radiative decays at LHCb

Search for $B^+ \to p\bar{\Lambda}^*(\to \bar{p}K^+)\gamma$

Jürgen F. Diverchy

Supervisor : Dr. Olivier Deschamps
Laboratoire de Physique de Clermont,
Université Clermont-Auvergne,
International Master of Advanced Methods in Particle Physics

Master's thesis presentation, 29th September 2025

Table of Contents

Table of Contents

The FCNC loop

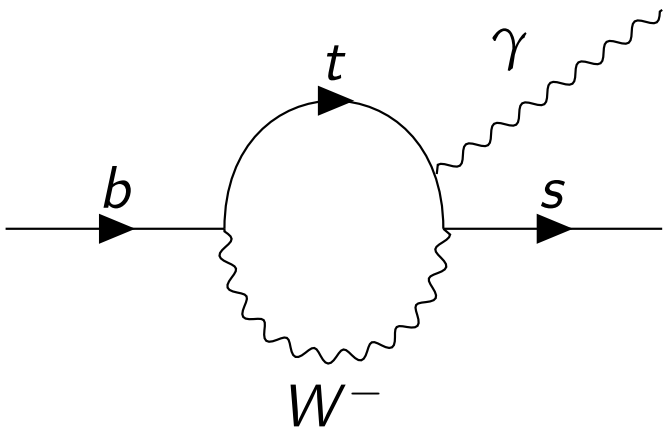

- In the SM, radiative decays of B mesons proceed via Flavour-Changing Neutral Currents (FCNC), occurring through loop transitions particularly sensitive to potential New Physics contributions.
- The aim of this search is to study the not observed yet decay $B^+ \to p\bar{\Lambda}^*\gamma$ with $\bar{\Lambda}^* \to \bar{p}K^+$.
- This preliminary study focuses on selecting $p\bar{p}K^+\gamma$ candidates and isolating the $B^+ \to p\bar{\Lambda}^*\gamma$ signal by modelizing the invariant mass spectrum, calibrating the PID and training a Boosted Decision Tree to suppress combinatorial background.

Studied decay $B^+ \to p\bar{\Lambda}^*\gamma$

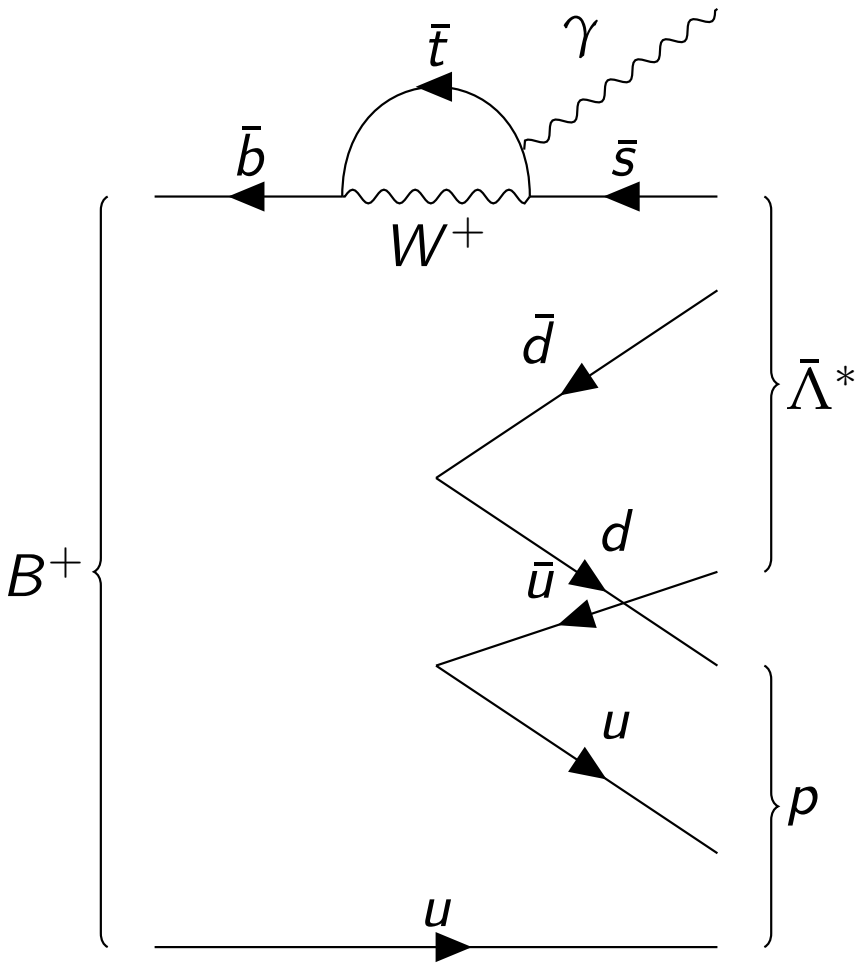

Theory

The radiative $B^+ \to p\bar{\Lambda}^*\gamma$ decay is a $\bar{b} \to \bar{s}\gamma$ FCNC transition. The photon is emitted from the loop involving heavy virtual particles, such as the top quark and the W boson. The $\bar{\Lambda}^*$ resonance decays into a K^+ and a $\bar{p}$ resulting into three charged tracks and an energetic photon in the final-state.

Despite the absence of prediction on this decay, we can make naive assumptions $\mathcal{B}(B^+ \to p\Lambda(1520)\gamma) \approx \frac{\mathcal{B}(B^+ \to p\Lambda(1115)\gamma)}{\mathcal{B}(B^+ \to p\Lambda(1115)} \times \mathcal{B}(B^+ \to p\Lambda(1520)) \approx (3.1 \pm 1.6) \times 10^{-6}$.

Experimental topology of the decay

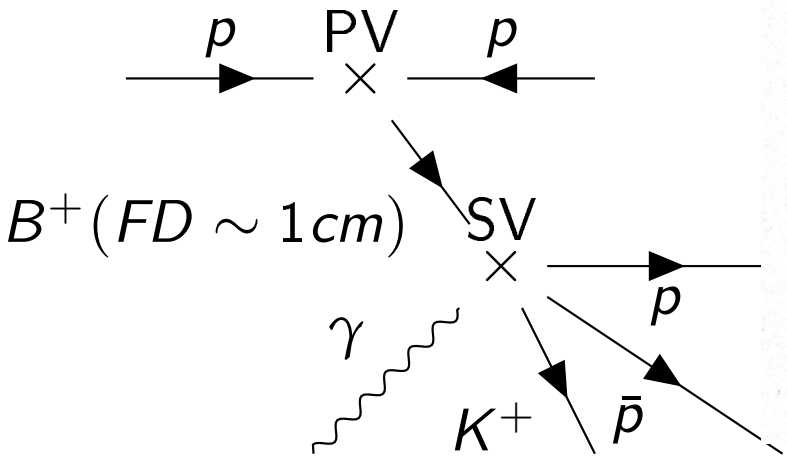

Schematic representation of the decay topology

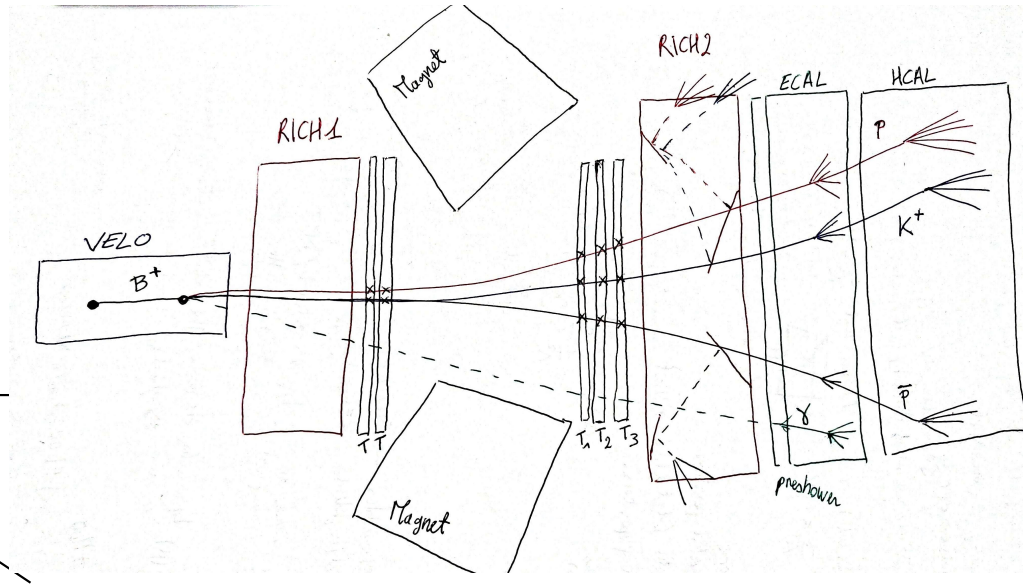

Schematic representation of the decay in the LHCb detector with the three charged tracks and the photon

Table of Contents

Trigger strategy

Trigger level	**Trigger requirement**
L0	`L0PhotonDecision` OR `L0ElectronDecision`
HLT1	`Hlt1TrackAllL0Decision` OR `Hlt1TrackPhotonDecision`
HLT2	Various radiative topo lines

Stripping line : StrippingB2XGamma3pi

Candidate	Selection
Pions	$p > 1\,GeV/c$ $p_T > 300\,MeV/c$ $\chi^2_{ndf} < 3$ Track minimum $\chi^2_{IP} > 16$ Track GhostProb < 0.4 $\sum p_T > 1.5\,GeV/c$
Photon	$p_T > 2\,GeV/c$
B meson	$2.9 \leq m_B \leq 9\,GeV/c^2$ $\sum_{Bdaughters} p_T > 5\,GeV/c^2$ $\chi^2_{vtx}/ndf < 9$ $\chi^2_{IP} < 9$

Offline pre-selection for $p\bar{p}K^+\gamma$

B candidate	$\theta_{Dira} < 0.06$ $p_T > 2 GeV/c$ $\chi^2_{IP} < 9.0$ Smallest $\Delta\chi^2$ one track > 3
Photon	$\gamma_{CL} > 0.2$ IsPhoton > 0.6 $p_T > 3 GeV/c$
Daughter Tracks (p,$\bar{p}$, K^+)	$\chi^2_{IP,min} > 20$ for all three tracks min$p_T > 500 MeV/c$ $p > 4.5 GeV/c$ and $p < 100 GeV/c$ $1.5 < \eta < 5.0$ for all three tracks
Vector candidate ($p\bar{\Lambda}^*$ system)	$\chi^2_{IP} > 0$ $\chi^2_{endvtx} < 9$ $m < 5.5 GeV/c^2$
PID	K^+ ProbNNk $>$ max(0.05, ProbNNpi, ProbNNp) $\bar{p}$, p ProbNNp $>$ max(0.05, ProbNNpi, ProbNNk)

Specific backgrounds

Combinatorial background
Partially reconstructed background
Track misidentification ($K\pi\pi\gamma$ or $KKK\gamma$) (negligible because of small branching fractions and reliance on double mis-ID)

Charmonia processes	**Branching Fraction**
$B^+ \to \eta_c K^+,\ \eta_c \to p\bar{p}\pi^0$	$3.74 \cdot 10^{-6}$
$B^+ \to J/\psi K^*(892)^+,\ J/\psi \to p\bar{p},\ K^*(892)^+ \to K^+\pi^0$	$1.01 \cdot 10^{-6}$
$B^+ \to J/\psi K^+,\ J/\psi \to p\bar{p}\pi^0$	$1.21 \cdot 10^{-6}$
$B^+ \to \eta_c K^*(892)^+,\ \eta_c \to p\bar{p},\ K^*(892)^+ \to K^+\pi^0$	$< 0.8 \cdot 10^{-6}$
$B^+ \to \chi_{c0} K^+,\ \chi_{c0} \to p\bar{p}\pi^0$	$3.32 \cdot 10^{-7}$
$B^+ \to \psi(2S) K^+,\ \psi(2S) \to p\bar{p}$	$1.8 \cdot 10^{-7}$
$B^+ \to \psi(2S) K^*(892)^+,\ \psi(2S) \to p\bar{p},\ K^*(892)^+ \to K^+\pi^0$	$0.65 \cdot 10^{-7}$
$B^+ \to \psi(2S) K^+,\ \psi(2S) \to p\bar{p}\pi^0$	$9.5 \cdot 10^{-8}$

Selection

$p\bar{p}K^+\gamma$ selection

- $m(p\bar{p}) < 2.9$ GeV to suppress η_c background
- $m(p\bar{p}\pi^0) > 3.2$ GeV to ensure the suppression of J/ψ
- $m(K^+\pi^0) > 2$ GeV to further ensure the suppression of charm(less) contaminations (aggressive cut killing the signal in half)

$J/\psi K^*(892)^+$ selection (preliminary control channels)

- We selected events consistent with $B^+ \to J/\psi K^*(892)^+$ using $m(p\bar{p})$ around J/ψ mass within 30 MeV and $m(K^+\pi^0) < 1.1$ GeV

Table of Contents

Monte Carlo samples at preselection level

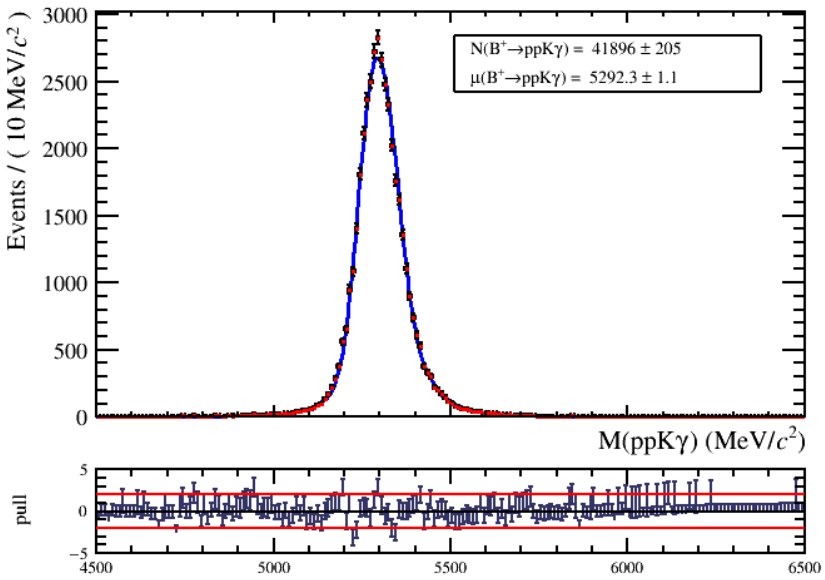

$B^+ \to p\bar{p}K^+\gamma$

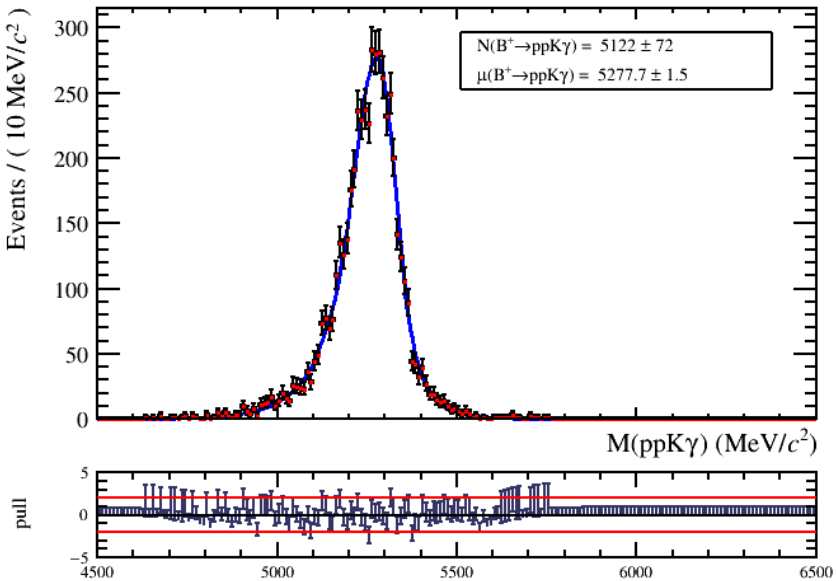

$B^+ \to J/\psi(\to p\bar{p})K^{*+}(\to K^+\pi^{\mathbf{0}})$

Control sample is obtained by applying the dedicated selection, with the photon substituted as a π^0.
All distributions are fitted with a Double-Sided Crystal Ball, the extracted parameters are later used to fit the signal in data.

$p\bar{p}K^+\gamma$ invariant mass fit after preselection

$\Rightarrow$ First ever observation of the $B^+ \to p\bar{p}K^+\gamma$ decay !

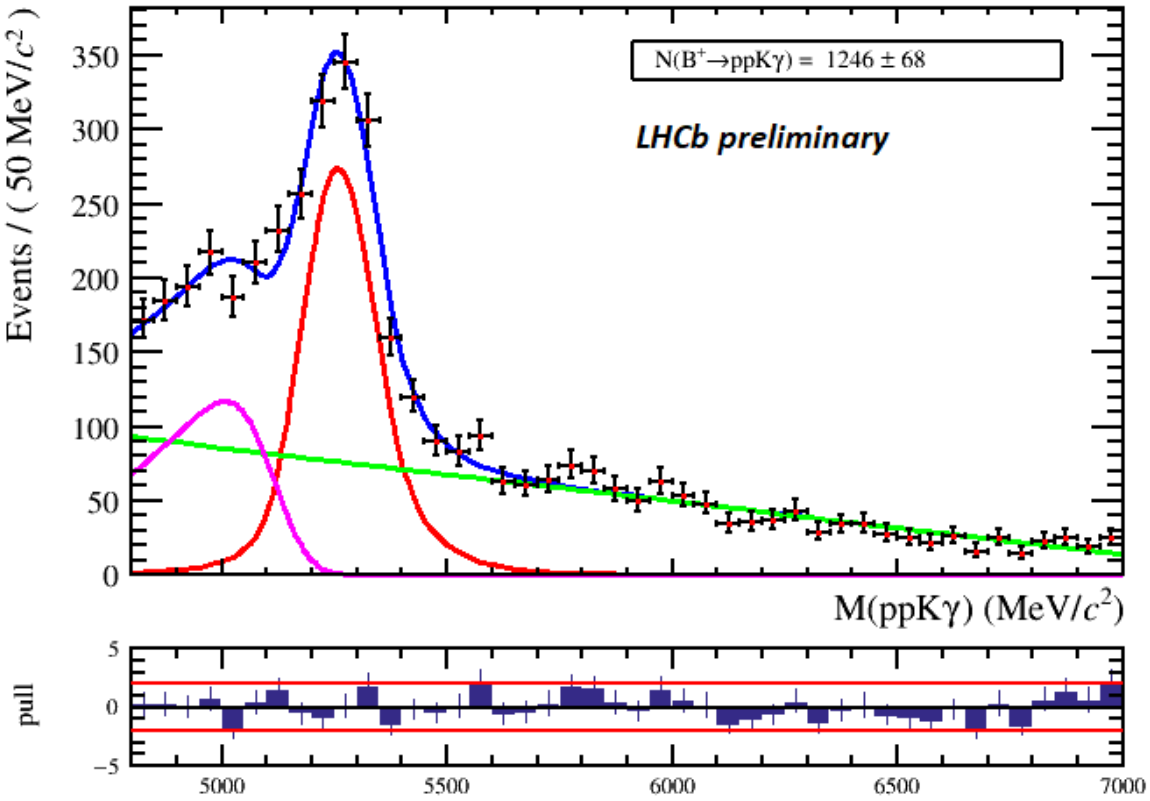

The total PDF consists of a signal component, partially reconstructed background, and combinatorial background.

Significance :
$Z \approx \frac{1246}{68} \approx 18\sigma$
Resolution :
$\sigma = 84 \pm 5 MeV/c^2$

$J/\psi K^*(892)^+$ invariant mass fit at preselection level

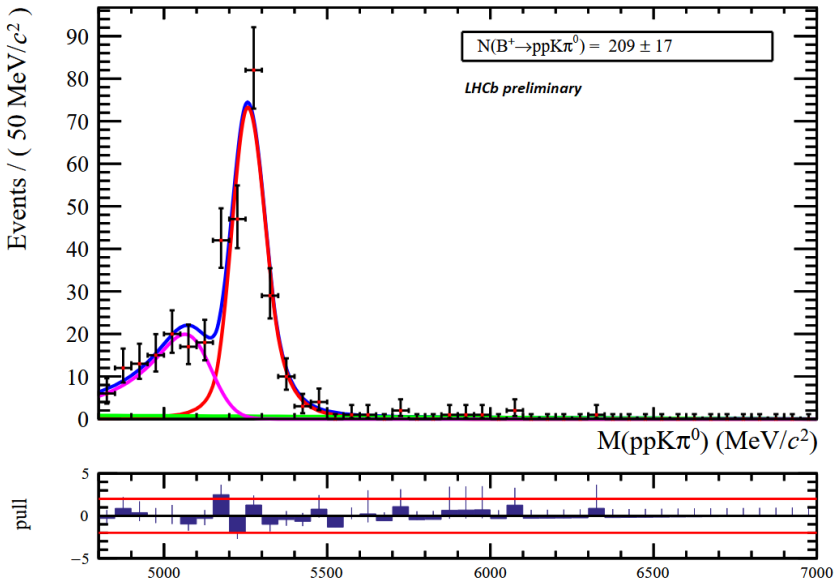

The total PDF consists of a signal component, partially reconstructed background, and combinatorial background.

This control fit was produced using the dedicated selection on $B^+ \to J/\psi K^*(892)^+$, with $J/\psi \to p\bar{p}$ and $K^*(892)^+ \to K^+\pi^0$. Each component of the total PDF was fitted using the same functions as the previous analysis, yielding 209 reference signal events.
This spectrum is almost combinatorial background-free.

Table of Contents

The PIDCalib2 package

Method

- Toolkit to determine PID efficiencies from real calibration samples.
- Uses high-statistics decays selected with minimal PID bias:

  Protons: $\Lambda^0 \to p\pi^-$, $\Lambda_c^+ \to pK^-\pi^+$,
  Kaons / Pions: $D^{*+} \to D^0(\to K^-\pi^+)\pi^+$.
- Efficiencies computed in bins of:

  Momentum $|\vec{p}|$,
  Pseudorapidity η,
  Track multiplicity n_{tracks}.
- Extracted with sPlot background subtraction $\to$ multidimensional histograms applied to signal tracks.

Binning schemes

- Calibration samples are non-uniform in $(|\vec{p}|, \eta, n_{\text{tracks}})$.
- Dense clusters $\rightarrow$ need fine binning, sparse regions $\rightarrow$ need wider bins.
- Legacy method: Urania bin-merging (isopopulation / uniform width) $\rightarrow$ produced pathological bins (zero events, efficiencies < 0 or > 1).
- Problems: thresholds arbitrary, ignored correlations, no handling of sWeights.
- A new 3D Bayesian binning method was developed during this internship to address these issues.

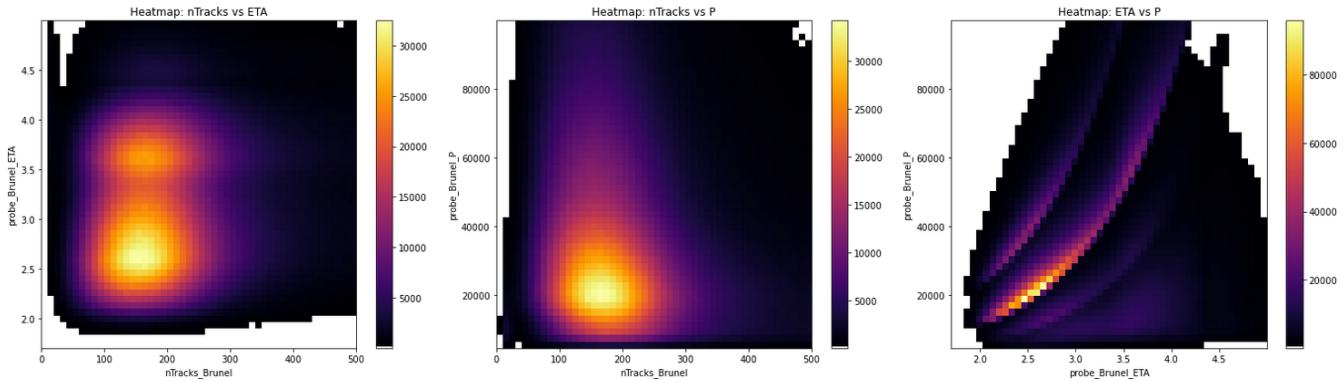

Figure: Distributions of the event density along the three calibration variables 2D projections for the 2015 (up polarity) proton samples. The white regions indicate little to no-event regions with less than 10 events

Tridimensional Bayesian binning method

Principle

- Goal: build an optimal binning scheme in $(|\vec{p}|, \eta, n_{\text{tracks}})$ that yields stable and unbiased PID efficiency estimates.
- Method: treat each bin b as a small statistical model with

$$n_b = \sum_{i \in b} w_i, \quad k_b = \sum_{i \in b \cap D_{\text{pass}}} w_i,$$

  where n_b is the weighted total and k_b the weighted passed counts.
- Likelihood: in each bin, the pass probability p_b is modeled with a (quasi-)binomial log-likelihood

$$\ell_b(p_b) = k_b \ln p_b + (n_b - k_b) \ln(1 - p_b).$$

- Concept: finer binning $\rightarrow$ more parameters, lower variance per bin; coarser binning $\rightarrow$ fewer parameters, but introduces bias.
- Solution: Bayesian model comparison balances both effects automatically, ensuring efficiencies remain in $[0, 1]$ and avoiding pathological bins.

Greedy Bayesian merging algorithm

Model comparison

- Partition $\mathcal{P}$ scored by Bayesian Information Criterion: $\mathrm{BIC}(\mathcal{P}) = -2\ell^*(\mathcal{P}) + K(\mathcal{P}) \ln N_{\mathrm{eff}}$.
- Candidate merge: two adjacent bins along one axis.
- Compute BIC change:$\Delta\mathrm{BIC} = -2\Delta\ell^* - \ln N_{\mathrm{eff}}$.
- Merge accepted if $\Delta\mathrm{BIC} < 0$ (posterior gain).
- Iteratively pick best merge $\rightarrow$ nested sequence of partitions with non-increasing BIC.

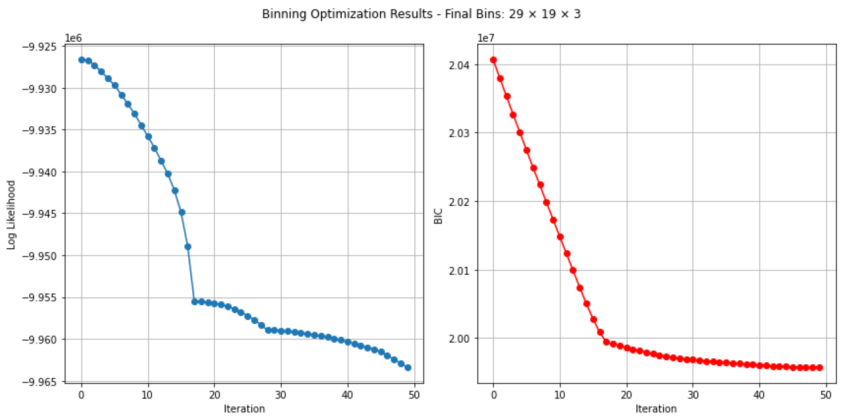

Variation of the log-likelihood (left) and BIC (right) in function of iterations of the binning scheme optimizer for the misidentification of pions into kaons on 2018 calibration files with polarity down.

Properties and practical implementation

Statistical features

- Automatic bias–variance trade-off: encoded in BIC penalty.
- Robust to sWeights: guarantees $0 \leq \hat{p}_b \leq 1$, avoids pathological bins.
- Objective: no ad hoc thresholds, purely evidence-based.
- Global hyperrectangular optimization : merges are evaluated simultaneously over all bins across the three observables, rather than restricting the search to one-dimensional projections. This holistic approach respects the true structure of the kinematic phase space (e.g. the absence of particles with simultaneously low momentum and high pseudorapidity).

Computational strategies

- Parallel evaluation of candidate merges (ThreadPoolExecutor).
- Memory-efficient: use of NumPy views, local likelihood updates.
- Early stopping when ΔBIC gain negligible.

Application to calibration samples

Procedure

- Applied to real calibration samples to extract PID efficiencies, independently for each year (2011, 2012, 2015–2018) and magnet polarity (up, down).
- PID requirement for kaon identification:

$$\text{ProbNNK} > max(\text{ProbNN}\pi, \text{ProbNNp}, 0.05)$$

(with analogous definitions for pion/proton by interchanging hypotheses).

- Weighted counts (n_b, k_b) obtained in each grid bin via sPlot subtraction, then merged with the Bayesian algorithm to optimize binning.

Outcome

- Resulting binning schemes implemented in `PIDCalib2` to produce efficiency histograms for reweighting $B^+ \to p\bar{p}K^+\gamma$ simulations.
- Calibration revealed significant $p, \bar{p} \to K$ mis-ID at $|\vec{p}| < 10$ GeV/c.
- $\to$ impose momentum requirement $p_{p,\bar{p}} > 10$ GeV/c to reduce cross-feed contamination.

Table of Contents

BDT training samples with extraction related to the preliminary fits

We designed a BDT with an optimized architecture to clean the combinatorial background on each year and runs to enhance the $B^+ \to p\bar{\Lambda}\gamma$ signal.

Signal

Signal events used in the training are taken from the Monte Carlo samples with $p\bar{p}K^+\gamma$ selection applied.

Background

Selected real data from the right-hand sideband (RHSB) region is used as background for the training, defined within the B^+ mass range [5.7;7] GeV/c^2. A looser PID cut has been applied on the background sideband to enhance statistics.

BDT training variables

Variable	Description
$\chi^2_{IP}(B)$	χ^2 increase of the primary vertex when adding the tracks of the reconstructed B^+ candidate
$p(B)$	Momentum of the reconstructed B^+ candidate
$f_D(B)$	Flight distance of the reconstructed B^+ candidate
Smallest $\Delta\chi^2_{vtx}(B)$	χ^2 of the vertex of the reconstructed B^+ candidate when adding an additional most compatible track
$\eta(B)$	Pseudorapidity of the reconstructed B^+ candidate
$\min(IP(p), IP(\bar{p}), IP(K^+))$	Minimum value of the impact parameter of the charged tracks
$p_T(p)$	Transverse momentum of the proton candidate
$p_T(\bar{p})$	Transverse momentum of the anti-proton candidate
$p_T(K^+)$	Transverse momentum of the K^+ candidate
Cone p_T asym (only available in Run 2)	Transverse momentum asymmetry in a cone around the B^+ momentum

n-fold method

All models were trained using a 2-fold cross-validation scheme to minimize overfitting and assess generalization.

Variables separation

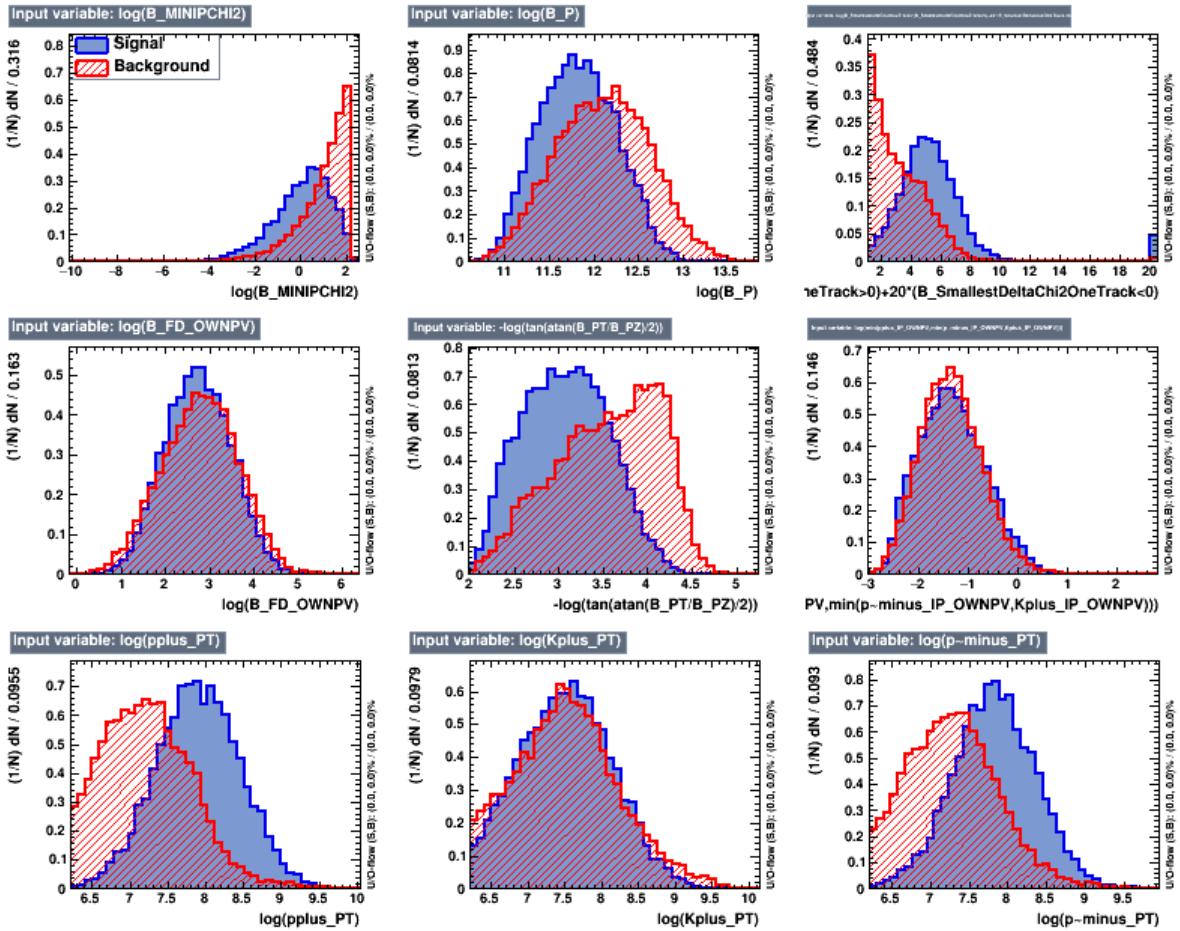

Distributions of the variables used in the training of the BDT for the Run 1 and Run 2 samples with RHSB background events (red) and MC signal events (blue).

Classification outputs

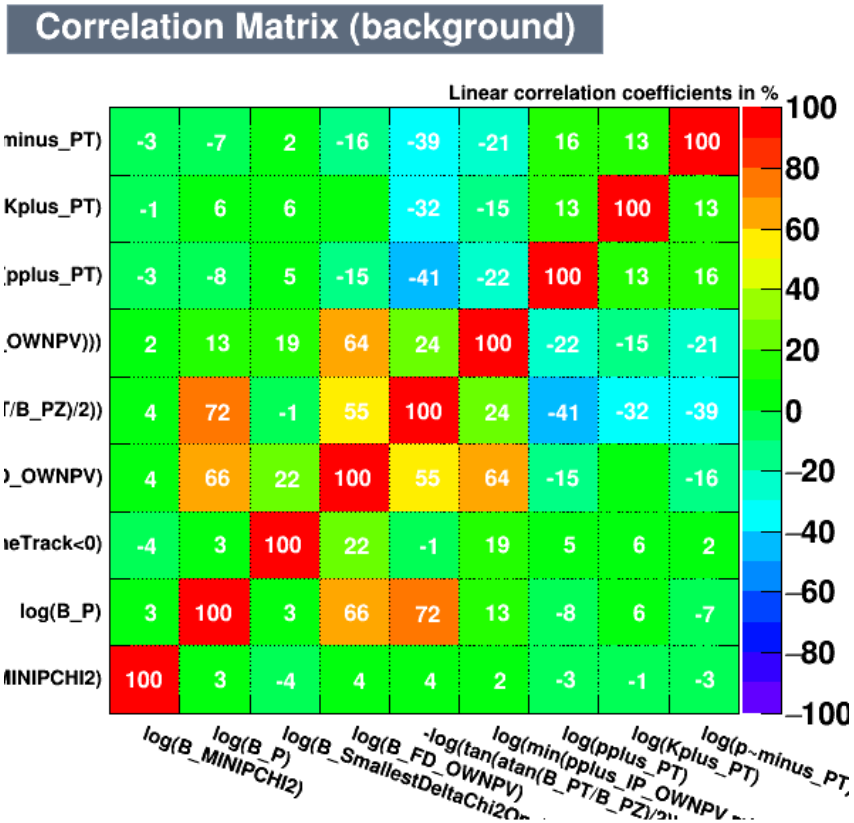

Correlations between BDT variables estimated with MC sample for Run 1 and Run 2 (the same plot exists for MC signal, with similar results).

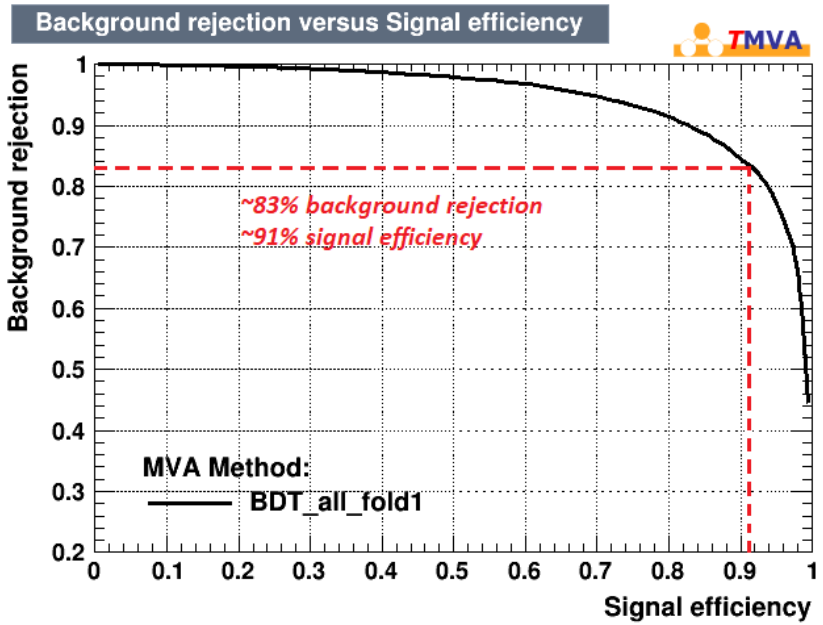

ROC curve output of the BDT classification for Run 1 and Run 2 sample.

Background estimation and figure of merit

Optimization of the BDT cut

The optimization procedure is implemented to determine the best cut value on the BDT output. The Punzi figure of merit is computed such as $FoM(\mathrm{BDT}) = \epsilon_{signal} / (\frac{\alpha}{2} + \sqrt{\frac{N_{bkg}^{3\sigma}}{N_{bkg}^{RHSB}} B_{comb}})$ with $\alpha = 3$, B_{comb} the number of combinatorial events in the RHSB passing the cut, N_{bkg}^{RHSB} the total number of events in the RHSB and $N_{bkg}^{3\sigma}$ the number of events extrapolated under the signal region.

Background estimation and figure of merit

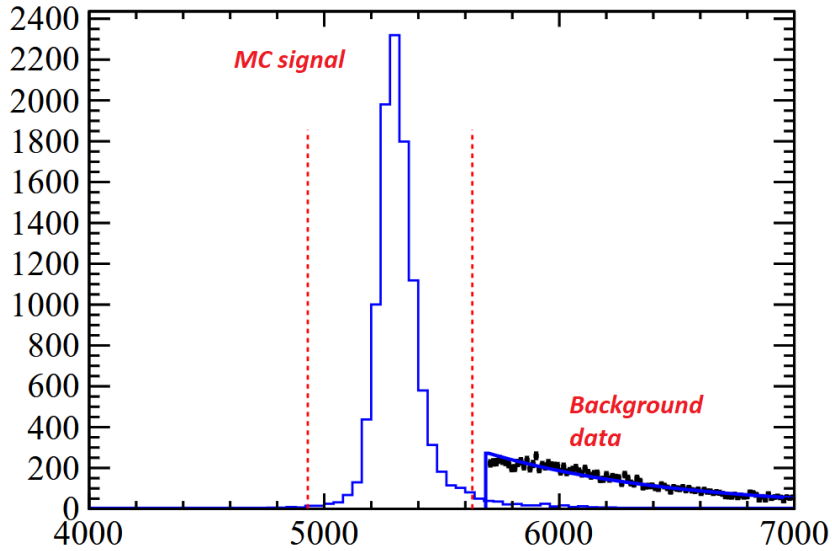

Histogram of the MC signal peak superposed with the fitted RHSB background data without BDT cut. The red lines represent the signal region where the fit is extrapolated.

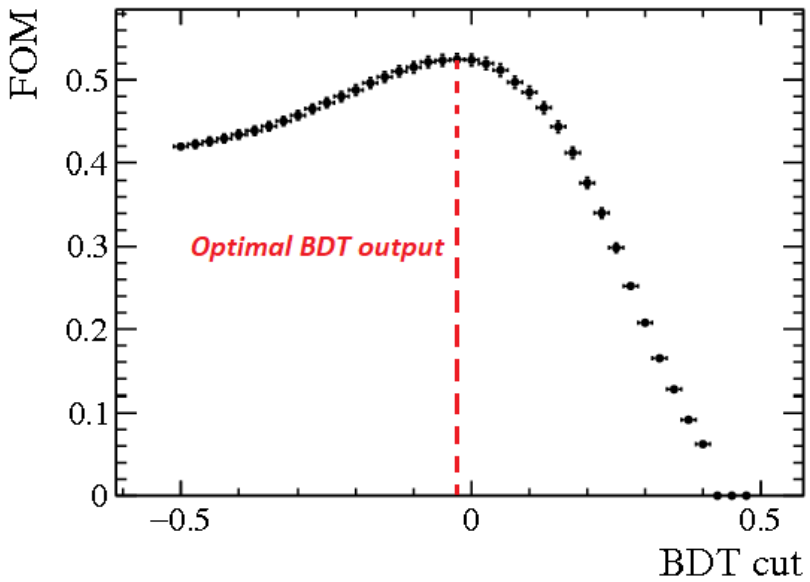

Punzi Figure of Merit against the BDT response.

$p\bar{p}K^+\gamma$ invariant mass fit after BDT cut

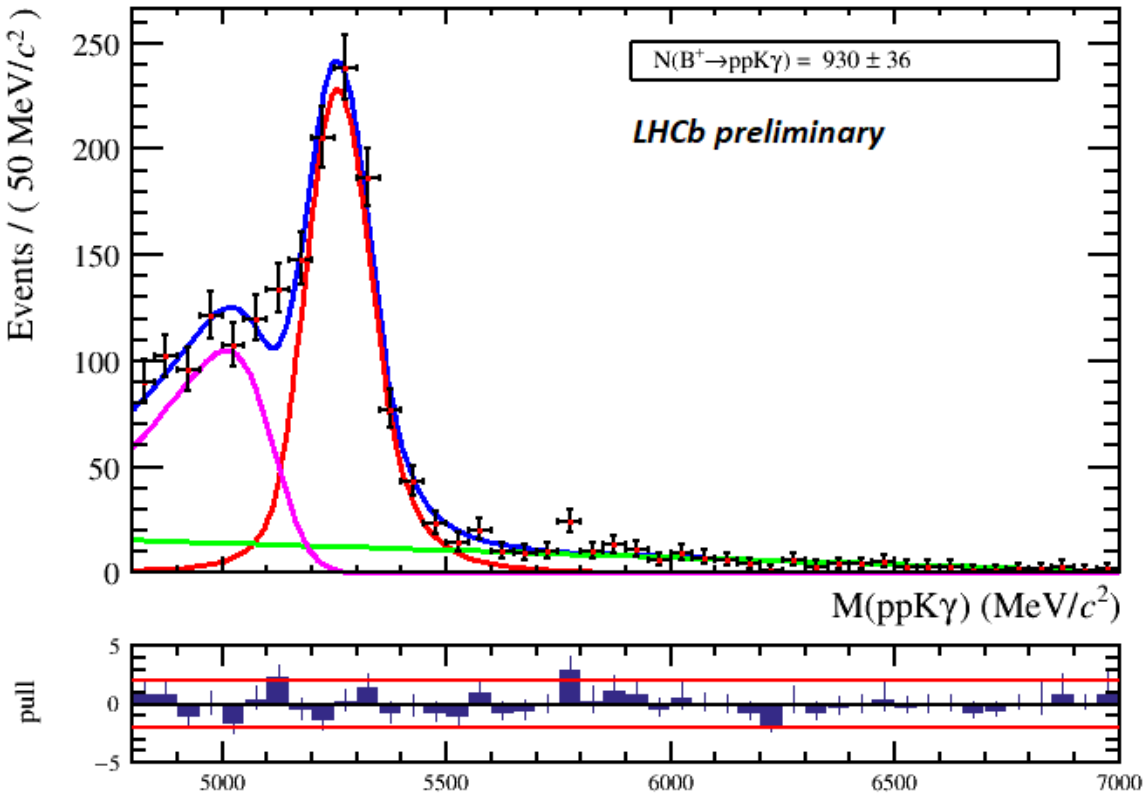

Preliminary fit to the $p\bar{p}K^+\gamma$ invariant mass spectrum after the application of the optimized MVA output. This fit will permit to extract the sWeights.

Significance :
$Z \approx \frac{930}{36} = 26\sigma$
Resolution :
$\sigma = 75.2 \pm 0.3 MeV/c^2$

Table of Contents

Selection Efficiencies

$$\varepsilon_{\text{tot}} = \varepsilon_{\text{gen}} \times \frac{N_{\text{presel}}}{N_{\text{gen}}} \times \frac{N_{\text{BDT}}}{N_{\text{presel}}} \times \frac{\sum_i w_{\text{PID}}}{N_{\text{BDT}}}$$

Year	$\varepsilon_{\text{gen}}(\%)$	$\varepsilon_{\text{presel}}(\%)$	$\varepsilon_{\text{BDT}}(\%)$	$\varepsilon_{\text{PID}}(\%)$	$\varepsilon_{\text{tot}}(\%)$
2011	21.130 ± 0.028	0.185 ± 0.004	81.8 ± 0.8	45.9 ± 1.2	0.0147 ± 0.0005
2012	21.400 ± 0.030	0.160 ± 0.003	79.5 ± 0.7	52.2 ± 0.9	0.0142 ± 0.0004
2017	22.210 ± 0.030	0.267 ± 0.004	85.4 ± 0.5	70.8 ± 0.7	0.0359 ± 0.0006
2018	22.190 ± 0.029	0.247 ± 0.003	79.3 ± 0.6	71.6 ± 0.7	0.0311 ± 0.0005
All	21.808 ± 0.059	0.218 ± 0.002	81.7 ± 0.3	64.1 ± 0.4	0.0240 ± 0.0003

Table: $B^+ \to p\bar{p}K^+\gamma$ *efficiencies.*

Branching ratio

Preliminary branching ratio estimation

The branching ratio of $B^+ \to p\bar{\Lambda}^*(\to \bar{p}K^+)\gamma$ is estimated using the normalization channel $B^+ \to J/\psi(\to p\bar{p})K^{*+}(\to K^+\pi^0)$.

$$\mathcal{B}_S = \mathcal{B}_N \times \frac{N_S}{N_N} \times \frac{\varepsilon_N}{\varepsilon_S},$$

where: $\mathcal{B}_S$: estimated branching ratio of the signal,

$\mathcal{B}_N = (1.01 \pm 0.0582) \times 10^{-6}$: visible branching ratio of the normalization channel,

$N_S = 930 \pm 36$: observed signal yield,

$N_N = 187 \pm 12$: observed normalization yield,

$\varepsilon_S = (2.4 \pm 0.03) \times 10^{-4}$: total efficiency of the signal,

$\varepsilon_N = (7.47 \pm 0.1) \times 10^{-5}$: total efficiency of the normalization channel.

$$\Rightarrow \mathcal{B}(B^+ \to p\bar{\Lambda}^*(\to \bar{p}K^+)\gamma) = (1.6 \pm 0.2) \times 10^{-6}$$

Table of Contents

Dibaryon spectrum

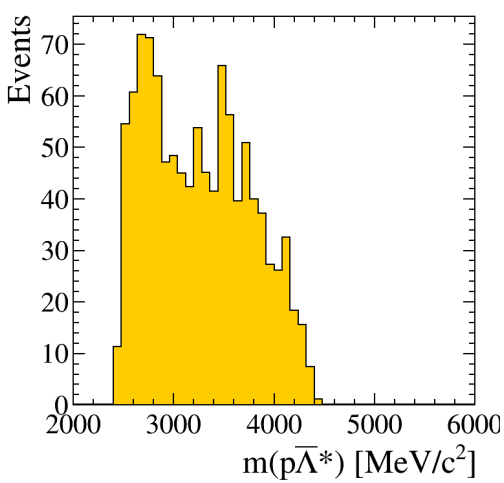

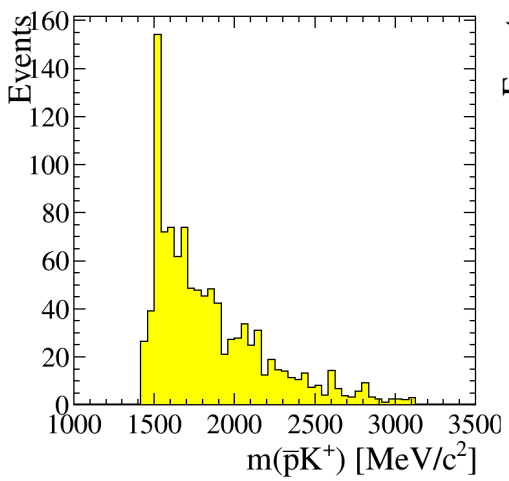

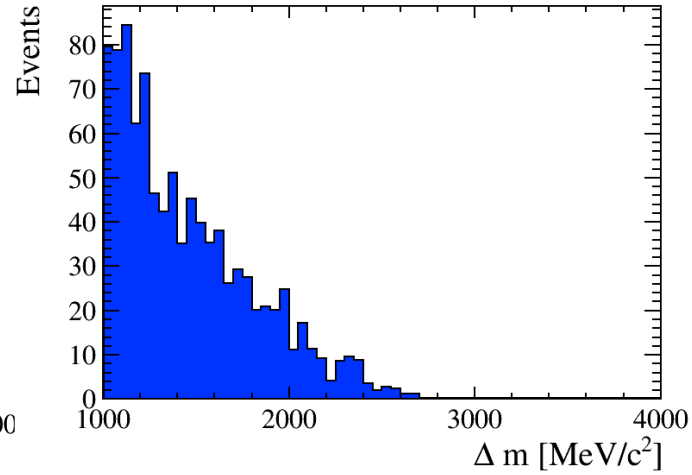

Reconstructed invariant masses of $p\bar{\Lambda}^*$ system and $\bar{\Lambda}^*$ state (and their difference) after combinatorial background removal and sWeights applied. No visible structure can be identified in the $p\bar{\Lambda}^*$ spectrum. Various baryons ($\Lambda(1520)$, $\Lambda(1670)$ ...) are distinguishable in the $\bar{\Lambda}^*$ mass spectrum.

Photon polarization measurement

The studied decay displays 3 charged tracks in the final state, allowing to extract the photon polarization from an angular analysis of the decay. The polarization is then quantified through up–down asymmetries with respect to the hadron decay planes, defined as $A_{ij} = \frac{N(\cos\theta_{ij}>0)-N(\cos\theta_{ij}<0)}{N(\cos\theta_{ij}>0)+N(\cos\theta_{ij}<0)}$.

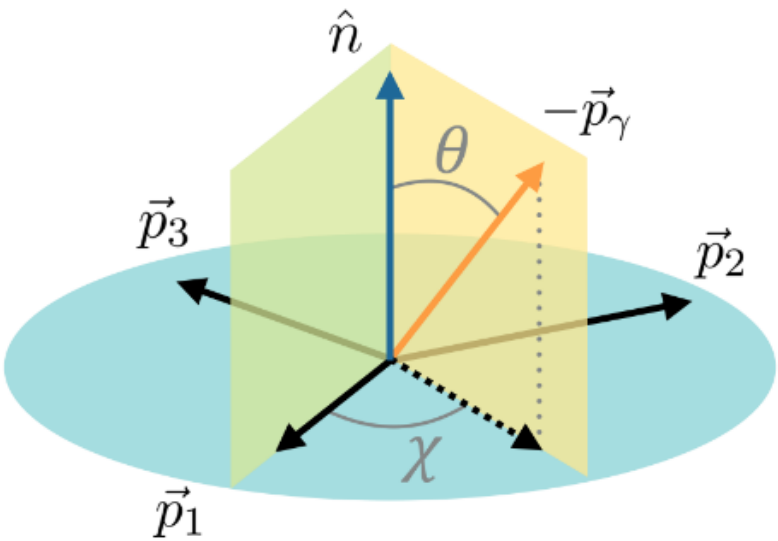

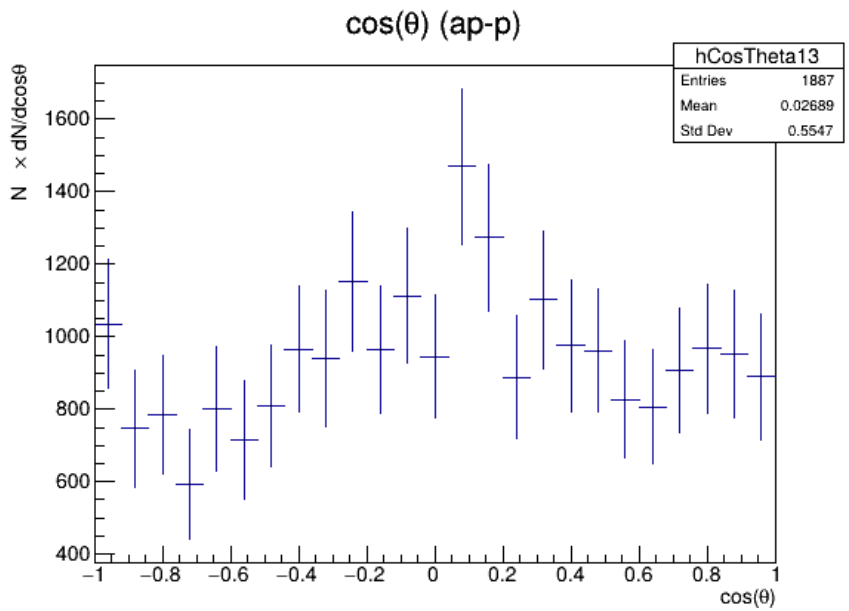

sWeighted angular distribution of the emitted photon with respect to the proton-antiproton plane in the $p\bar{\Lambda}^*$ rest frame.

Table of Contents

Summary

Main results and contributions

- **Selection** : Selection of $p\bar{p}K^+\gamma$ candidates and isolation of the $B^+ \to p\bar{\Lambda}^*\gamma$ signal in the invariant mass spectrum,
- **PID calibration**: Development of a novel 3D Bayesian binning algorithm for PID efficiency estimation,
- **Background suppression**: Training and optimization of a BDT to reduce combinatorial background,
- **First observation** of $B^+ \to p\bar{p}K^+\gamma$ decay with high significance (26σ),
- **Branching fraction estimation**: $\mathcal{B} = (1.6 \pm 0.2) \times 10^{-6}$.

Future prospects

To-do list

- Preliminary control channel $J/\psi K^{(*)+}$ rely on π^0/γ separation and display low statistics,
- Study of track mis-ID low background contamination,
- $K\pi\pi\gamma$ display larger statistics but relies on precise control of double mis-ID, it may be used for better branching ratio estimation,
- For the normalization, the possibility to use $B^+ \to J/\psi K^+$ samples, with J/ψ decaying into $p\bar{p}\pi^0$ or $p\bar{p}\gamma$ is currently under study,
- Branching fraction measurement systematic uncertainties,
- Amplitude analysis to separate $\bar{\Lambda}^*$ resonances,
- Photon polarization measurement and helicity coefficient extraction.

Thank you for your attention !

Selection of control channel

$J/\psi K^+$ selection (preliminary control channels)

- We selected $m(p\bar{p}\pi^0)$ candidates around the J/ψ mass within 75 MeV to isolate the peak for control

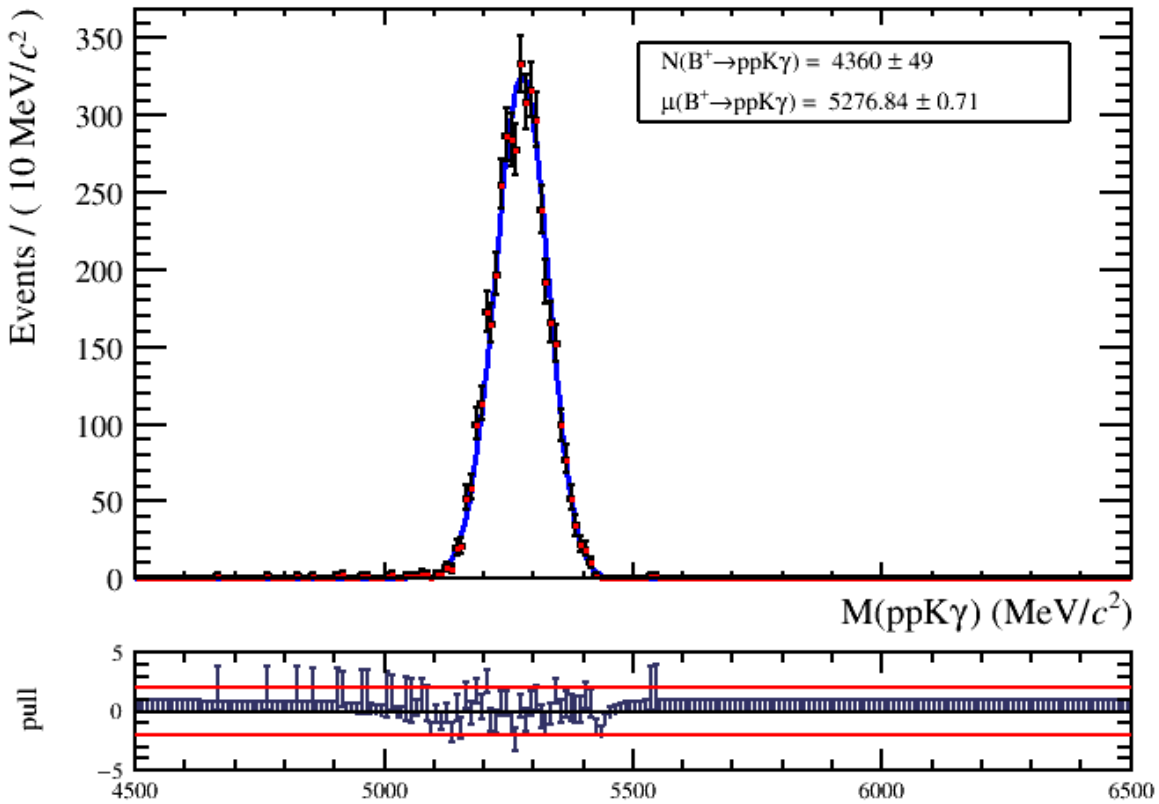

$J/\psi K^+$ invariant mass fit at preselection level

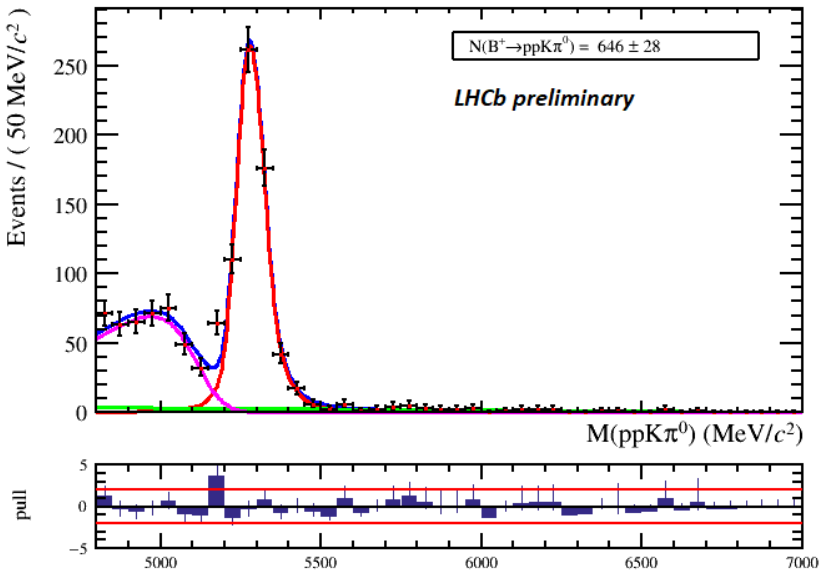

The total PDF consists of a signal component, partially reconstructed background, and combinatorial background.

This control fit was produced using the dedicated selection on $B^+ \to J/\psi K^+$, with $J/\psi \to p\bar{p}\pi^0$. Each component of the total PDF was fitted using the same functions as the previous analysis, yielding 646 reference signal events, that could be used for future normalization.
This spectrum is almost combinatorial background-free.

Control samples invariant mass fit after PID cut

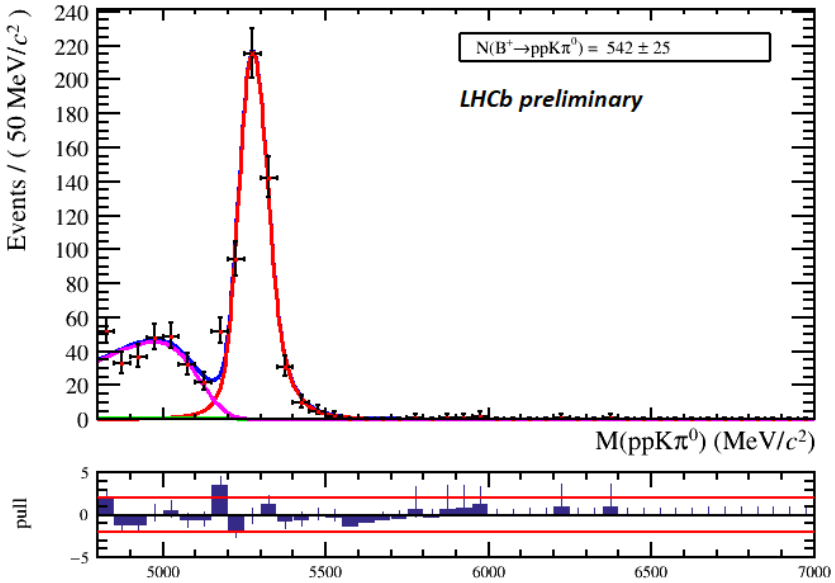

Preliminary fit to $B^+ \to J/\psi(\to p\bar{p}\pi^0)K^+$ invariant mass spectrum.

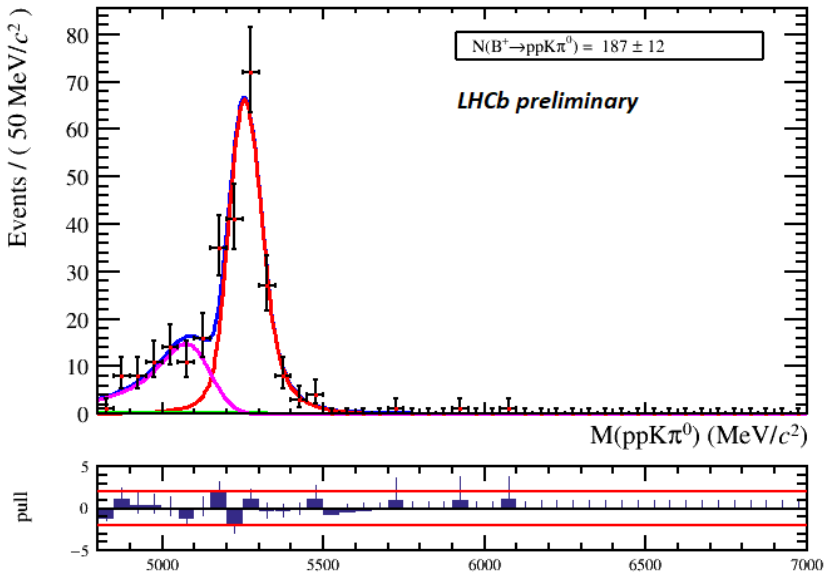

Preliminary fit to $B^+ \to J/\psi(\to p\bar{p})K^{*+}(\to K^+\pi^0)$ invariant mass.

Excess in the $J/\psi K^+$ sample

Observation

Despite the fact that $\mathcal{B}(B^+ \to J/\psi(\to p\bar{p}\pi^0)K^+) = 1.21 \times 10^{-6}$ and $\mathcal{B}(B^+ \to J/\psi(\to p\bar{p})K^{*+}(\to K^+\pi^0)) = 1.01 \times 10^{-6}$, it can be seen that there are 2.9 times more events in the fitted $J/\psi(\to p\bar{p}\pi^0)K^+$ than in the $J/\psi(\to p\bar{p})K^{*+}(\to K^+\pi^0)$ sample.
It will be seen later that their reconstruction efficiency is similar.

Hypothesis

The $J/\psi \to p\bar{p}\gamma$ process was not taken into account because of its smaller branching ratio ($\mathcal{B}(J/\psi \to p\bar{p}\gamma) = 3.8 \times 10^{-4}$) with respect to $J/\psi \to p\bar{p}\pi^0$ ($\mathcal{B}(J/\psi \to p\bar{p}\pi^0) = 2.12 \times 10^{-3}$), but the reconstruction efficiency of $J/\psi \to p\bar{p}\gamma$ is likely to be larger than the one of $J/\psi \to p\bar{p}\pi^0$, resulting in these discrepancies.

Cluster mass distribution

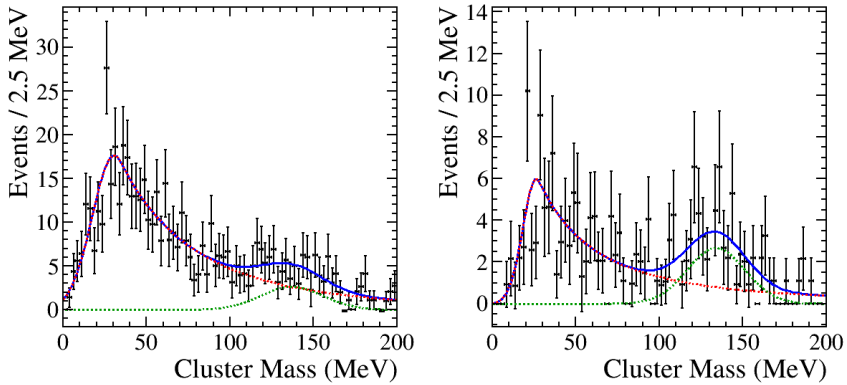

Fit to cluster mass distribution of $J/\psi(\to p\bar{p}\pi^0)K^+$ (left) and $J/\psi(\to p\bar{p})K^{*+}(\to K^+\pi^0)$ (right). The model (blue) consists of a Crystal Ball merged component (red dashed) and a Gaussian resolved component (green dashed).

Analysis of the excess

In the $J/\psi(\to p\bar{p})K^{*+}$ channel the two contributions are clearly separated, while in $J/\psi(\to p\bar{p}\pi^0)K^+$ about two thirds of the events are described by the Crystal Ball component, with a much smaller resolved part. This suggests a significant contribution from $J/\psi \to p\bar{p}\gamma$, enhanced by its harder photon spectrum compared to π^0.

Hypothesis status

This interpretation remains a hypothesis. A dedicated Monte Carlo study including $J/\psi \to p\bar{p}\gamma$ is required to assess efficiencies and confirm whether this effect explains the observed discrepancy.

Selection Efficiencies of control samples

Year	$\varepsilon_{\mathbf{gen}}$	$\varepsilon_{\mathbf{presel}}$	$\varepsilon_{\mathbf{BDT}}$	$\varepsilon_{\mathbf{PID}}$	$\varepsilon_{\mathbf{tot}}$
2011	$16.380 \pm 0.029\%$	$0.0381 \pm 0.002\%$	$83.2 \pm 1.81\%$	$51.5 \pm 2.65\%$	$0.00267 \pm 0.0002\%$
2012	$16.730 \pm 0.032\%$	$0.0271 \pm 0.001\%$	$80.1 \pm 1.62\%$	$57.2 \pm 2.24\%$	$0.00208 \pm 0.0001\%$
2017	$17.700 \pm 0.031\%$	$0.0765 \pm 0.002\%$	$89.2 \pm 0.711\%$	$79.2 \pm 0.985\%$	$0.00957 \pm 0.0003\%$
2018	$17.670 \pm 0.031\%$	$0.0631 \pm 0.002\%$	$85.2 \pm 0.944\%$	$80.9 \pm 1.13\%$	$0.00768 \pm 0.0003\%$
All	$17.240 \pm 0.062\%$	$0.0538 \pm 0.001\%$	$86.1 \pm 0.524\%$	$74.3 \pm 0.713\%$	$0.00593 \pm 0.0001\%$

Table: $B^+ \to J/\psi(\to p\bar{p}\pi^0)K^+$ *efficiencies.*

Year	$\varepsilon_{\mathbf{gen}}$	$\varepsilon_{\mathbf{presel}}$	$\varepsilon_{\mathbf{BDT}}$	$\varepsilon_{\mathbf{PID}}$	$\varepsilon_{\mathbf{tot}}$
2011	$16.780 \pm 0.033\%$	$0.0437 \pm 0.002\%$	$88.4 \pm 1.45\%$	$52.0 \pm 2.40\%$	$0.00337 \pm 0.0002\%$
2012	$17.040 \pm 0.032\%$	$0.0317 \pm 0.001\%$	$90.3 \pm 1.11\%$	$59.6 \pm 1.93\%$	$0.00291 \pm 0.0001\%$
2017	$18.040 \pm 0.032\%$	$0.0916 \pm 0.002\%$	$91.2 \pm 0.623\%$	$79.2 \pm 0.934\%$	$0.0119 \pm 0.0003\%$
2018	$17.980 \pm 0.032\%$	$0.0808 \pm 0.002\%$	$85.4 \pm 0.829\%$	$80.2 \pm 1.01\%$	$0.00995 \pm 0.0003\%$
All	$17.558 \pm 0.065\%$	$0.0650 \pm 0.001\%$	$88.2 \pm 0.451\%$	$74.1 \pm 0.652\%$	$0.00747 \pm 0.0001\%$

Table: $B^+ \to J/\psi(\to p\bar{p})K^{*+}(\to K^+\pi^0)$ *efficiencies.*

The LHCb detector

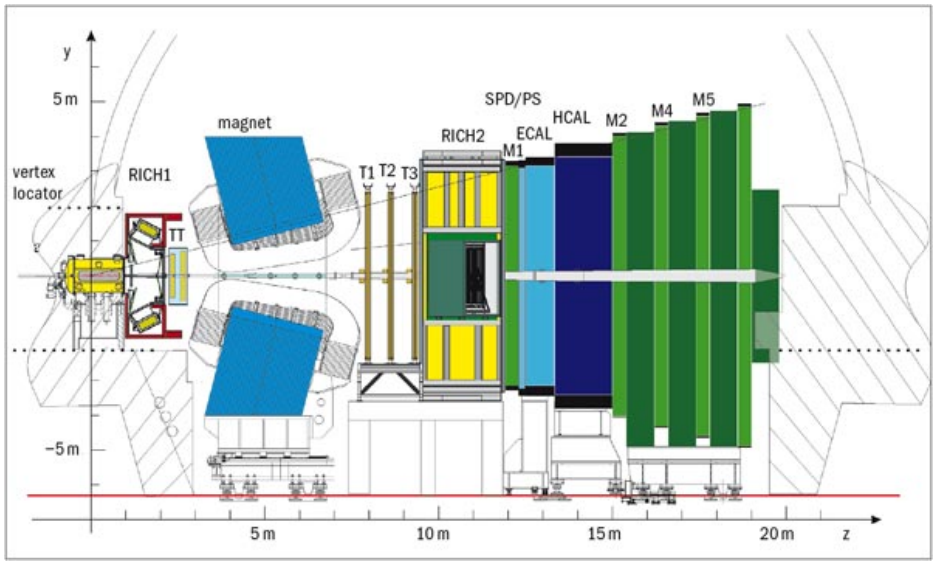

Schematic view of the LHCb detector

- **VELO** : Silicon detector identifying primary and secondary vertices.
- **Trackers** : Devices reconstructing the charged proton and kaon tracks.
- **RICH** : Detectors identifying charged particles (proton/kaon separation) thanks to Cherenkov radiation.
- **Calorimeter system** : ECAL reconstructs radiated photon momentum by absorbing its energy and producing a shower of secondary particles. HCAL absorbs and measures the energy of hadrons by detecting hadronic showers.

Efficiency distributions for PID calibration

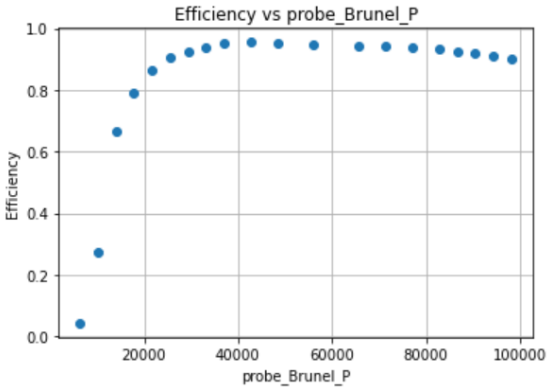

Variation of PID efficiency in function of momentum

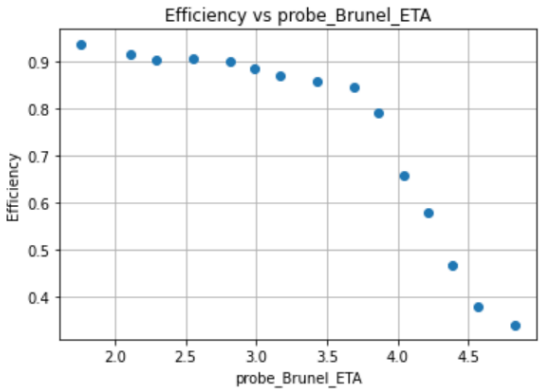

Variation of PID efficiency in function of pseudorapidity

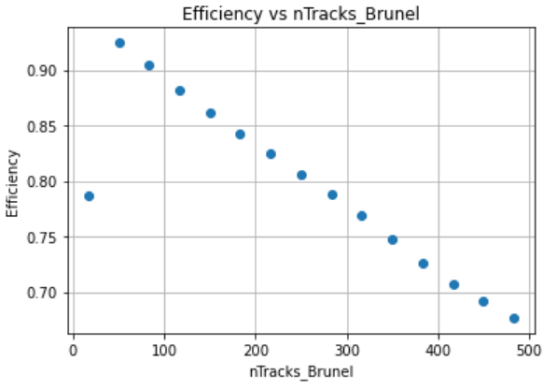

Variation of PID efficiency in function of track multipicity

Decision trees architecture

The Boosted Decision Tree (BDT) training in this analysis is implemented using the TMVA framework with the following common setup across all datasets:

- **Boosting Algorithm:** AdaBoost
- **Max Tree Depth:** 3
- **Bagging:** Enabled with a sample fraction of 60%
- **Number of Cuts:** 20 per feature

Year	2011	2012	2017	2018	Run 1	Run 2	All
Number of trees	200	300	800	800	500	1700	1700
Minimum Node Size	5 %	3 %	2.5 %	2.5 %	2.5 %	2.5 %	2.5 %

Monte Carlo samples after BDT and PID calibration

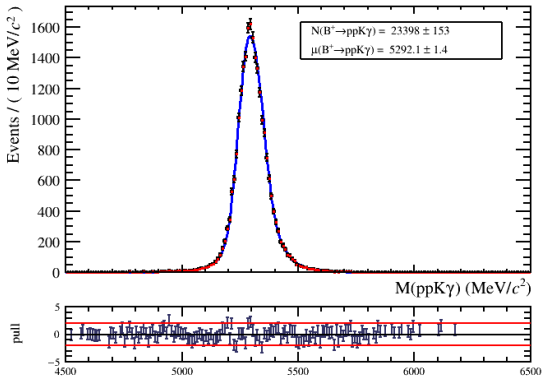

$B^+ \to p\bar{p}K^+\gamma$

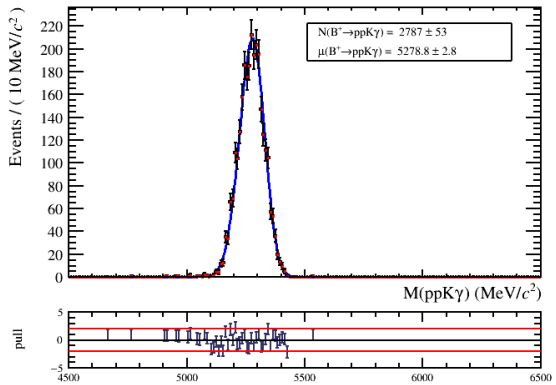

$B^+ \to J/\psi(\to p\bar{p}\pi^0)K^+$

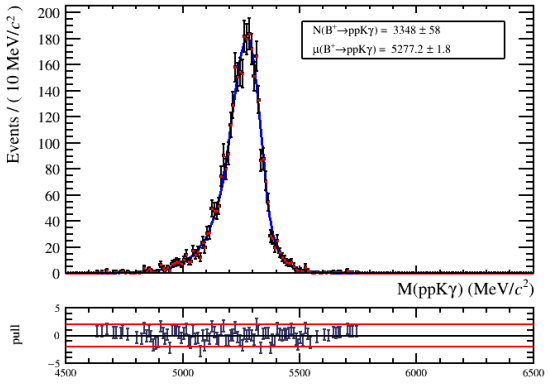

$B^+ \to J/\psi(\to p\bar{p})K^{*+}(\to K^+\pi^0)$

Control samples are obtained by a dedicated selection.
All distributions are fitted with a Double-Sided Crystal Ball, the extracted parameters are later used to fit the signal in data.

Photon angular distributions

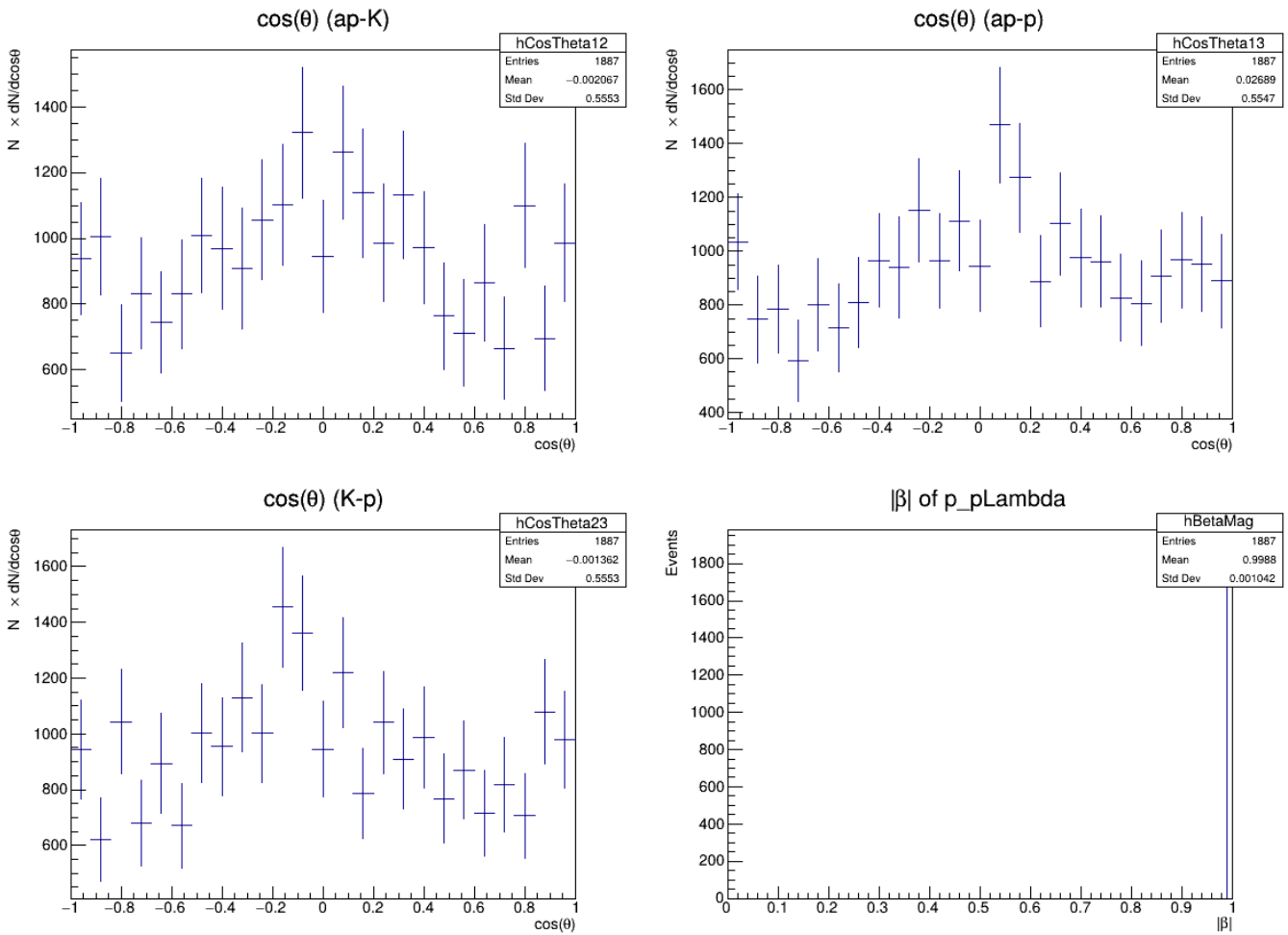

sWeighted angular distribution of the emitted photon with respect to each plane in the $p\bar{\Lambda}^*$ rest frame and β of this system.